Enhancing Detection of Acceleration-Related ERPs in VR using Spatial Filtering Techniques

Gaël Van der Lee, François Cabestaing, Hakim Si-Mohammed
Univ. Lille, CNRS, Centrale Lille, UMR 9189
CRIStAL, F-59000, Lille, France
Emails: gael.vanderlee@univ-lille.fr, francois.cabestaing@univ-lille.fr, hakim.simohammed@univ-lille.fr

***Abstract*—Decoding user perception in Virtual Reality (VR) is crucial for enhancing immersion and understanding the user experience. This study compared spatial filtering techniques for enhancing acceleration-related ERPs from EEG data in VR. Participants experienced controlled forward and backward accelerations within a VR environment while their brain activity was recorded using a 14-electrode EEG system. We compare spatial filtering methods—CSP, EMS, and xDAWN—and demonstrate that xDAWN most effectively separates these acceleration conditions. These findings provide insights into the neural mechanisms underlying acceleration perception in VR, paving the way for improved VR experiences and a deeper understanding of the brain processes associated with acceleration perception.**

***Index Terms*—EEG, acceleration detection, spatial filter.**

I. Introduction

Electroencephalography (EEG) offers a non-invasive window into brain activity with unparalleled temporal resolution, making it an invaluable tool for studying dynamic neural processes. Of particular interest in EEG research are Event Related Potentials (ERPs), which are neuromarkers evoked by an external event. However, raw EEG signals are often obscured by noise, volume conduction, and cross-channel correlations, presenting a significant challenge in isolating meaningful neural activity. In our preceding work [1], we found novel neural markers associated with acceleration and its direction by analyzing specific electrodes.

Notably, we discovered a significant difference between perceived forward and backward acceleration at the Cz electrode signal, as well as through manual combinations of multiple signals at neighboring electrodes. Building upon these findings, this study investigates whether linear spatial filtering methods can effectively discriminate acceleration-related EEG signals. To this end, we employ a pipeline combining Independent Component Analysis (ICA) [2] with established linear spatial filtering techniques: Common Spatial Patterns (CSP) [3], Effect-Matched Spatial filtering (EMS) [4], and xDAWN [5]. By leveraging these filters, we seek to gain deeper insights into the brain's activation patterns during acceleration.

To achieve this goal, we first explore Common Spatial Patterns (CSP), a technique widely used for extracting discriminative spatial filters that maximize variance differences between two conditions in multi-sensor neural data [3]. CSP optimally decomposes EEG signals into spatial components that best separate experimental conditions by enhancing specific signal variance in one condition while minimizing variance in the other. It has been widely used in motor imagery classification, cognitive state decoding, and clinical applications such as seizure detection [6]. It is particularly effective in motor imagery tasks but is sensitive to inter-trial variability and noise.

Next, we consider Effect-Matched Spatial (EMS) filtering, a technique that extracts a single representative time course from multi-sensor neural recordings by dynamically adjusting a spatial filter at each time point [4]. This approach maximizes the signal-to-noise ratio (SNR) while preserving interpretability. Using leave-one-out cross-validation, EMS filtering prevents circularity and ensures unbiased extraction of experimental effects. Unlike PCA or ICA, which capture fixed spatial patterns, EMS filtering directly tracks evolving neural responses. It has been shown to improve single-trial detection and has been applied successfully in cognitive and motor studies.

Finally, we examine the xDAWN algorithm, a spatial filtering technique developed to enhance ERPs, particularly the P300 component, in EEG data [5]. In Brain-Computer Interface (BCI) applications, such as the P300 speller paradigm introduced by Farwell and Donchin [7], users focus on target stimuli that elicit P300 responses, enabling communication without muscular activity. However, P300 signals are often obscured by background EEG activity and noise. The xDAWN algorithm addresses this challenge by estimating spatial filters that maximize the signal-to-signal-plus-noise ratio, effectively enhancing the ERP component.

Despite the widespread adoption of these techniques in different EEG contexts, their relative performance in the context of VR-induced ERPs remains unexplored. This is particularly relevant given the challenges of EEG in VR, such as increased motion artifacts, nonstationary signal properties, and the need for feature extraction methods that generalize across varying stimulus conditions. Understanding how these spatial filtering techniques compare in enhancing EEG features during VR experiences is crucial for optimizing ERP-based VR research and applications. Therefore, this study aims to directly compare these filters in the context of EEG-based VR acceleration perception. We evaluate their performance by assessing (1) filter output separability via bootstrapping and (2) multi-dimensional discriminability using Linear Discriminant Analysis.

The remainder of this paper is structured as follows: section II details the EEG data acquisition, experimental setup, and preprocessing. section III presents the evaluation methods, results, and discussion. section IV presents and discusses the results.

II. Methodology

A. Data Acquisition and Experimental Setup

EEG data was collected using OpenVibe 3.1.0 software and a g.GAMMAcap2 EEG cap from g.tec medical engineering GmbH®(Austria) with 15 electrodes positioned at FPz, Fz, F1, F2, FCz, FC1, FC2, Cz, C1, C2, CPz, CP1, CP2, Pz and a reference electrode placed on the right earlobe. The virtual environment was created using the Unity game engine software (version 2020.3.11f1), featuring a virtual scene composed of point clouds and a central crosshair.

Thirty healthy participants with normal or corrected to normal vision took part in the experiment (18 men, 12 women aged $\mu = 26$, $min = 18$, $max = 56$, $\sigma = 7.38$). We extended the experimental setup from our previous work [1]. Participants were exposed to a virtual environment (VE) simulating forward and backward motion. Each 17-second trial consisted of four phases. First, a 2-second *Static* phase established the visual scene followed by a *Slow speed* phase, where the environment moved at a constant $3m/s$ for a duration of 1 to 5 seconds, providing a baseline visual stimulus. Next, the *Acceleration* phase involved a 1-second acceleration of $12m/s^2$, either forward (FA) or backward (BA). The resulting velocity was maintained for 2 seconds, followed by a return to $3m/s$. Finally, an *End* phase maintained the $3m/s$ speed for a duration matching the slow speed phase before fading out over 2 seconds.

The VE comprised a minimalist scene of white spheres arranged cylindrically, with participants fixating on a central red crosshair. Spheres appeared gradually from a distance of 150 meters and were updated in real time based on the simulated speed. Participants completed 78 trials, divided into four blocks, with balanced conditions (forward/backward accelerations and variable durations). This protocol was approved by the University of Lille's ethics committee with approval number 2021-526-S97.

B. Preprocessing

We first visually identify noisy channels[1] and exclude them participant-wise. We implement a notch windowed FIR filter at 50 Hz to eliminate power line interference from the recordings. Following ERP literature [8], data are filtered in the 0.3 to 10 Hz range using a 4th order IIR forward and backward Butterworth filter and resampled to 50 Hz. Each trial is divided into epochs starting from 0.5 seconds before the acceleration onset and lasting until 1 second after it. Similarly to noisy channels, epochs with overwhelming noise or eye blink artifacts are removed.

We then use ICA [2] to remove artifacts generated by eye blinks, manually identifying and removing noise and artifact components from the data. Following ICA, we apply baseline correction for each epoch from -0.4 to 0 seconds. These epochs are stored and used for analysis.

In the following, tensors are denoted by underlined bold uppercase letters ($\underline{\boldsymbol{V}}$), matrices by bold uppercase letters ($\boldsymbol{X}$), column vectors by bold lowercase letters ($\boldsymbol{w}$), fixed scalars by cursive uppercase letters (C), variable scalars by cursive lowercase letters (f) and methods or conditions in typewriter font (CSP, FA).

Let $\underline{\boldsymbol{X}} \in \mathbb{R}^{E \times S \times C}$ denote the EEG data tensor, where E is the number of epochs, S the number of samples per epoch, and C the number of channels. Each observation is a channel vector $\boldsymbol{x}_{e,s} \in \mathbb{R}^C$ in an epoch $e \in [0..E-1]$ for a sample $s \in [0..S-1]$. We denote E_{FA} and E_{BA} the number of epochs associated with conditions FA and BA, respectively ($E = E_{\text{FA}} + E_{\text{BA}}$). After preprocessing, we have $E_{\text{FA}} = 1127$ corresponding to $\underline{\boldsymbol{X}}_{\text{FA}}$ and $E_{\text{BA}} = 1113$ corresponding to $\underline{\boldsymbol{X}}_{\text{BA}}$, i.e. $\underline{\boldsymbol{X}}_{\text{FA}} \in \mathbb{R}^{E_{\text{FA}} \times S \times C}$ and $\underline{\boldsymbol{X}}_{\text{BA}} \in \mathbb{R}^{E_{\text{BA}} \times S \times C}$.

C. Spatial filtering and analysis

A spatial filter is defined as $\boldsymbol{w} \in \mathbb{R}^C$, implementing a linear mapping $\mathbb{R}^C \to \mathbb{R}$, yielding the virtual electrode output $v_{e,s} = \boldsymbol{x}_{e,s}^\top \boldsymbol{w}$. A set of F spatial filters forms a matrix $\boldsymbol{W} \in \mathbb{R}^{C \times F}$, yielding the virtual electrode vector $\boldsymbol{v}_{e,s} = \boldsymbol{x}_{e,s}^\top \boldsymbol{W} \in \mathbb{R}^F$. We denote the f-th spatial filter from method M as $\boldsymbol{w}_{\text{M},f} = (\boldsymbol{W}_{\text{M}})_{:,f}$, where $f \in [1..F]$ and $\text{M} \in \{\text{AVG}, \text{CSP}, \text{EMS}, \text{xDAWN}\}$. The virtual electrode signal for a given method M is then denoted as:

$$\begin{cases} \boldsymbol{V}_{\text{M}} = \underline{\boldsymbol{X}} \boldsymbol{w}_{\text{M}} \in \mathbb{R}^{E \times S} & \text{if } F = 1 \\ \underline{\boldsymbol{V}}_{\text{M}} = \underline{\boldsymbol{X}} \boldsymbol{W}_{\text{M}} \in \mathbb{R}^{E \times S \times F} & \text{if } F > 1 \end{cases}$$

We denote the virtual electrode corresponding to the f-th spatial filter from method M as $\boldsymbol{V}_{\text{M},f} = (\underline{\boldsymbol{V}}_{\text{M}})_{:,f}$. The average spatial filter is defined as $\boldsymbol{w}_{\text{AVG}} = \frac{1}{C}\mathbf{1}$, where $\mathbf{1} \in \mathbb{R}^C$ is the vector of ones. Applied to each observation $\boldsymbol{x}_{e,s}$, it computes the mean across all channels. We apply the average and each of the 3 following filters separately on the data.

1) Common Spatial Pattern: For our two-condition problem with data $\underline{\boldsymbol{X}}_{\text{FA}}$ and $\underline{\boldsymbol{X}}_{\text{BA}}$, CSP seeks to find F spatial filters, with $F \in \{1, 2, 4\}$ in our implementation, which are a subset in $\mathbb{R}^{C \times F}$ of the full filter matrix $\boldsymbol{W}_{\text{CSP}} \in \mathbb{R}^{C \times C}$, that maximizes the objective function J:

$$J(\boldsymbol{W}_{\text{CSP}}) = \frac{\boldsymbol{W}_{\text{CSP}}^\top \boldsymbol{\Sigma}_{\text{FA}} \boldsymbol{W}_{\text{CSP}}}{\boldsymbol{W}_{\text{CSP}}^\top \boldsymbol{\Sigma}_{\text{BA}} \boldsymbol{W}_{\text{CSP}}} \tag{1}$$

where $\boldsymbol{\Sigma}_{\text{FA}}$ and $\boldsymbol{\Sigma}_{\text{BA}}$ are the spatial covariance matrices for the FA and BA conditions [3]. This objective function is solved as a generalized eigenvalue problem. We keep the top and bottom eigenvectors because the largest and smallest eigenvalues correspond to spatial filters that maximize variance for one condition while minimizing it for the other, capturing the most discriminative information. More CSP components are selected by alternating between the first and last eigenvectors as the number of filters, F, increases.

The projection of the EEG data onto these spatial filters yields virtual electrodes with maximal discriminability between the two conditions. For visualization in Figure 1, we use $F = 1$ to highlight the primary spatial pattern. For signal discrimination in Figure 3, we evaluate separability using $F \in \{1, 2, 4\}$ to assess the impact of additional filters. It is important to note that CSP is optimally suited for oscillatory or sustained power differences between conditions, rather than short, phase-locked ERP differences.

[1]Channels with excessive amplitude or overwhelming noise.

2) Effect-Matched-Spatial Filtering: Unlike other spatial filtering methods that focus on maximizing variance or specific frequency components, EMS is designed to optimize the extraction of experimental effects. The core principle of EMS filtering is to project data, at every sampling time, onto a single spatial filter that maximizes a specific objective function, most commonly the difference between two experimental conditions. EMS computes a separate spatial filter for each sample of the data, denoted $\boldsymbol{w}_{\texttt{EMS},s}$. The optimization problem is solved as follows:

$$\boldsymbol{w}_{\texttt{EMS},s} = \frac{\sum_{e=0}^{E-1} y_e \boldsymbol{x}_{e,s}}{\| \sum_{e=0}^{E-1} y_e \boldsymbol{x}_{e,s} \|} \tag{2}$$

where y_e is the label for epoch e, taking $1/E_{\texttt{FA}}$ if epoch e belongs to condition FA, and $-1/E_{\texttt{BA}}$ if it belongs to condition BA. $\boldsymbol{w}_{\texttt{EMS},s} \in \mathbb{R}^C$ is equivalent to the normalized difference between the mean response in condition FA and the mean response in condition BA at each sample [4]. To obtain a single filter for comparative visualization of all methods, we compute the mean $\boldsymbol{w}_{\texttt{EMS}} = \frac{1}{S}\sum_{s=0}^{S-1} \boldsymbol{w}_{\texttt{EMS},s} \in \mathbb{R}^C$. For evaluating separability, we use both the average filter $\boldsymbol{w}_{\texttt{EMS}}$ and one filter per sample using $\boldsymbol{w}_{\texttt{EMS},s}$.

3) xDAWN Spatial Filter: xDAWN utilizes the occurrence of the stimuli to enhance the signal-to-noise ratio. Here we apply xDAWN and create filters for each of the two conditions (FA and BA) separately. xDAWN first estimates the ERP responses, using least squares: $\hat{\mathbf{A}} = (\mathbf{D}^\top\mathbf{D})^{-1}\mathbf{D}^\top\underline{\boldsymbol{X}}$ with $\mathbf{D} \in \mathbb{R}^{S\times 2}$ a Toeplitz matrix encoding the stimulus onsets corresponding to the two conditions. Then, it designs spatial filters $\mathbf{U}$ that maximize the signal to signal-plus-noise ratio where $\mathbf{U} \in \mathbb{R}^{C\times C}$ is the matrix of all spatial filters, of which we keep a reduced filter matrix of size $\mathbb{R}^{C\times F}$.

Finally, the xDawn filter, $\boldsymbol{W}_{\texttt{xDAWN}}$, is estimated as:

$$\boldsymbol{W}_{\texttt{xDAWN}} = \arg\max_{\mathbf{U}} \frac{\text{Tr}(\mathbf{U}^\top\hat{\mathbf{A}}^\top\mathbf{D}^\top\mathbf{D}\hat{\mathbf{A}}\mathbf{U})}{\text{Tr}(\mathbf{U}^\top\underline{\boldsymbol{X}}^\top\underline{\boldsymbol{X}}\mathbf{U})} \tag{3}$$

where $\text{Tr}(\cdot)$ is the trace operator [5]. This optimization problem can be efficiently solved through QR decomposition and singular value decomposition. Separability is computed using $F \in \{1, 2, 4\}$ and visualization using $F = 1$.

III. Results & Discussion

A. Evoked potentials

We analyze the impact of individual spatial filters on the temporal evolution of signal amplitudes. When several filters can be determined, we just keep the most significant ($F = 1$), and compute the 95% confidence interval across epochs. 95% confidence intervals are shown around the response for each condition FA and BA using a non-parametric bootstrapping approach on 10,000 resamples on our data with replacement. Looking at the average of all electrodes for both conditions Figure 1 (a), we find a distinct signal consistent with the results found in [1]. There is a different signal when looking at the average of all electrodes in each condition FA and BA.

The CSP algorithm highlights only the component that encodes the most variance (first component) and effectively modulates the variance of the time series data, increasing variance for the FA condition and decreasing it for the BA condition, as seen in Figure 1 (b). However, this variance maximization approach did not optimize ERP separability because, in our paradigm, the main discriminative information is a polarity difference in the phase-locked ERP around Cz, not a sustained change in variance. CSP is designed to maximize variance differences, and is thus suboptimal for brief, phase-locked ERP components where opposite-polarity deflections result in similar variances across conditions. The resulting spatial filter predominantly isolated the signal from the Cz electrode (Figure 1 (f)). This observation aligns with our previous findings [1], where the Cz electrode was manually found to represent the most pronounced amplitude difference between the FA and BA conditions, suggesting that CSP, in this instance, effectively and automatically identified the electrode with the greatest discriminatory power, albeit not necessarily leading to optimal ERP separability in terms of signal difference.

The CSP-induced modulation of signal variance, specifically the increase in variance for one condition and the decrease for the other, manifests as a discernible difference in the time-frequency representation (TFR). This suggests that CSP effectively alters the frequency content of the signal in a condition-dependent manner. Figure 2 shows the significant clusters when looking at the difference of the TFR representation of FA and BA, with a stronger low frequency response (under 6Hz) between 200ms to 600ms after stimulus onset for FA. Time-frequency representations were computed using Morlet wavelets across a logarithmically-spaced frequency range from 1 to 10 Hz (50 frequency points), with the number of cycles adaptively scaled to optimize temporal and frequency resolution. The data were baseline-corrected using a log-ratio transformation relative to the pre-stimulus interval (-0.45 to -0.05 seconds).

To identify statistically significant differences between conditions, we employ a cluster-based permutation approach with 100 permutations and a threshold value of 6.0 from the literature [9]. This non-parametric statistical method effectively controls for multiple comparisons while taking into account the temporal and spectral adjacency of the time-frequency points. The analysis yields clusters of significant differences ($p \leq 0.05$) between conditions, visualized in Figure 2 using a bidirectional color map overlaid on the raw F-statistics, providing a comprehensive view of both statistical significance and effect directionality across the time-frequency space.

Looking at the result of the average EMS filter $\boldsymbol{V}_{\texttt{EMS}}$ shown in Figure 1(c), EMS appears to primarily invert the original signal, maintaining a near-uniform negative value across all electrodes, as shown in its filter in Figure 1 (g). It seems that the EMS filter does not enhance condition separation by differentially weighting electrodes, and assigns nearly equal weight across channels and samples, resulting in a global inversion. A likely explanation is that the unfiltered data already exhibits a difference between conditions, the EMS filter did not succeed in making this difference more pronounced. Because $\boldsymbol{w}_{\texttt{EMS},s}$ is estimated independently at every sample, the method

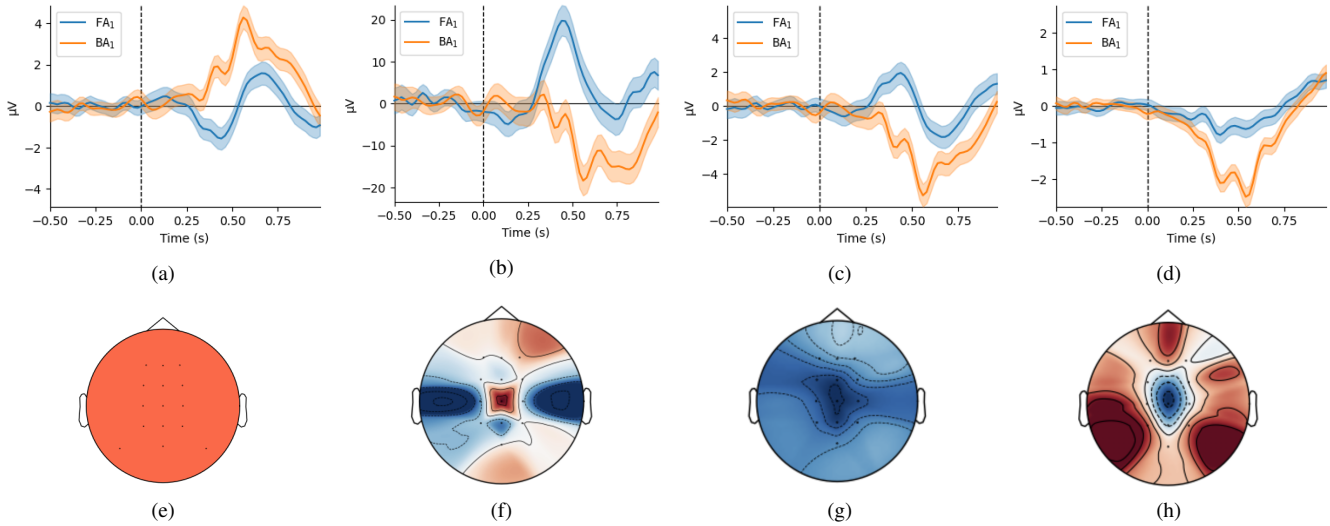

Fig. 1: First line: average evoked responses in the two conditions FA and BA for signals filtered by (a) the mean filter yielding $\boldsymbol{V}_{\text{AVG}}$, (b) the first CSP filter yielding $\boldsymbol{V}_{\text{CSP},1}$, (c) the average EMS filter yielding $\boldsymbol{V}_{\text{EMS}}$, and (d) the first xDAWN filter yielding $\boldsymbol{V}_{\text{xDAWN},1}$. Shaded areas indicate the 95% confidence interval over all epochs ($E_{\text{FA}} = 1127$, $E_{\text{BA}} = 1113$). Second line: spatial representation of the filters for (e) The average filter $\boldsymbol{w}_{\text{AVG}}$ yielding responses in (a), (f) the first filter for CSP $\boldsymbol{w}_{\text{CSP},1}$, (g) the average EMS filter $\boldsymbol{w}_{\text{EMS}}$, (h) the first xDAWN filter $\boldsymbol{w}_{\text{xDAWN},1}$.

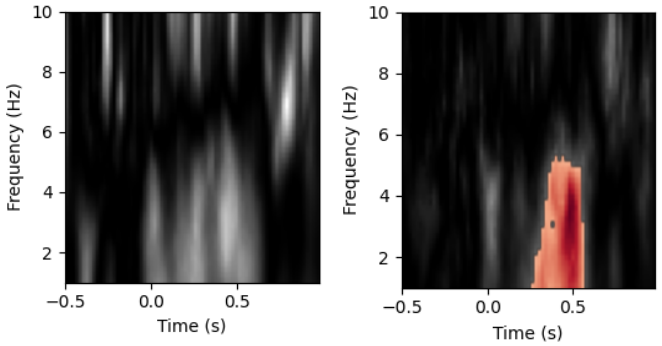

(a) Original data TFR significant clusters

(b) CSP significant clusters

Fig. 2: (a) Difference (FA vs. BA) of the average time frequency representation (TFR) of each condition. Significant ($p < 0.05$) clusters are only present in (b), with red representing a stronger signal in that band for the FA condition.

does not enforce any relationship between successive filters. When looking into individual time series, we observed that small fluctuations can flip the sign of $\boldsymbol{w}_{\text{EMS},s}$ from one sample to the next, yielding an erratic sequence of spatial patterns. This "sign-flipping" may cancel out slower ERP components that can only be seen when the whole epoch is considered jointly. Moreover, even when examining the sample-resolved EMS filters, the spatial filter remains relatively uniform and constant with negative values after $t = 0.2s$.

Finally, the xDAWN seems to yield superior separability between the FA and BA events compared to CSP and EMS (Figure 1 (d)). The selected filter maximizes the SNR for BA. The resulting signal exhibits a strong negative peak throughout the observed epoch, and effectively minimizes the FA amplitude. The spatial patterns associated with xDAWN reveal a specific topographical weighting (Figure 1 (h)). The selected filter is strongly weighted by a negative component centered on the Cz electrode, with the surrounding electrodes having positive weights, isolating the signal of interest and effectively minimizing the other condition. This improved performance is likely attributable to xDAWN's design, which is specifically tailored to enhance the signal-to-noise ratio of ERPs and maximize the discriminability between different ERP conditions, unlike CSP and EMS which optimize for variance or reconstruction error, respectively.

B. Condition-Separability Analysis

Filter performance is also assessed via a quantitative metric of condition separability. We employ Linear Discriminant Analysis (LDA) not to maximize absolute accuracy, but to provide a standardized, interpretable metric for comparing the separability achieved by each filtering method across different numbers of filters and training epochs. This approach enables quantitative evaluation of filter performance beyond visual inspection, allowing comparison in higher-dimensional feature spaces. We use a stratified k-fold cross-validation procedure (k=5) to ensure robust and unbiased assessment. For each spatial filter method (Average, CSP, xDAWN, and EMS), a two-stage pipeline is implemented: first, the spatial filter is fit to the training data and applied to the training set. A LDA model is then fitted on this output. Then the testing set is used for evaluating the filter. The stratification in the cross-validation procedure preserved the proportion of samples

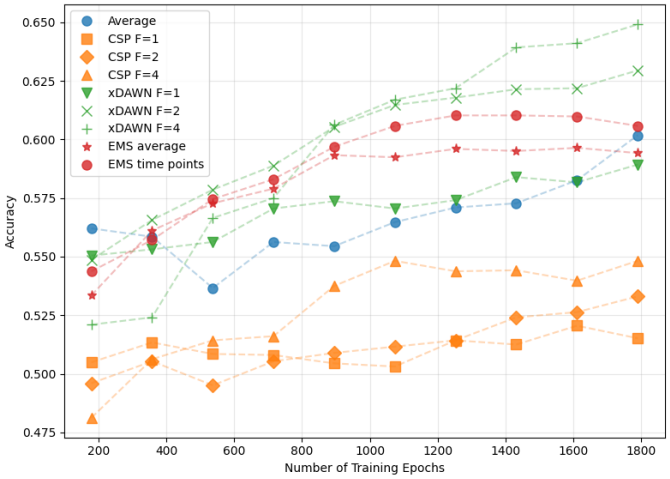

Fig. 3: Condition separability (measured by LDA accuracy) over number of training epochs for each spatial filter. The Average filter is compared to CSP with $F \in \{1, 2, 4\}$, to xDAWN with $F \in \{1, 2, 4\}$ and to EMS with one filter per sample or the average filter of all samples applied to the whole time series ($\boldsymbol{w}_{\text{EMS}}$ or $\boldsymbol{w}_{\text{EMS},s}$).

for each condition across folds, ensuring balanced evaluation. Curves of class separability were generated by incrementally increasing the number of epochs used for model fitting in ten equal steps, while maintaining the complete test set for evaluation. Each filter is evaluated across multiple settings as described in subsection II-C. Namely 1, 2 and $F = 4$ filters for xDAWN and CSP, and 1 or S filters for EMS. Class separability results can be found in Figure 3.

The separability of features extracted by CSP yields significantly lower accuracy compared to EMS, xDAWN, and the average. Among the tested methods, xDAWN achieved the highest condition separability, a finding that corroborates the enhanced ERP separability observed in the evoked potential plots in Figure 1. xDAWN performance improved significantly when fitting more than one filter. This allows the method to fit one filter per condition, and maximize the SNR for each condition independently, resulting in more distinguishable features. These results provide further quantitative evidence that xDAWN effectively enhances the discriminability of event-related potential signals, leading to improved separation between the `FA` and `BA` conditions. EMS exhibited strong performance, particularly with a lower number of epochs, matching xDAWN and surpassing it for $F = 1$. However, it did not scale as effectively and plateaued as the filter is applied to larger datasets.

CSP did not perform as well as the other filters. This might be due to the fact that the effectiveness of CSP relies on the assumption that the discriminative information between conditions is primarily contained in the variance of the signals rather than in their temporal patterns or phase relationships. This makes CSP particularly well-suited for analyzing oscillatory neural activity but potentially less effective for event-related potentials where temporal dynamics are critical.

All three spatial filtering techniques demonstrate high computational efficiency, with inference requiring only a matrix-vector multiplication, making them highly suitable for real-time applications. Furthermore, training these filters is also feasible for online scenarios: processing all 2240 epochs on an Apple M1 processor took 1.03 s for xDAWN, 1.10 s for CSP, and 1.55 s for EMS.

IV. Conclusion

This study performed a systematic comparison of spatial filtering techniques for enhancing acceleration-related ERPs from EEG data in VR. xDAWN outperformed CSP and EMS in ERP class separability. While EMS was not the most efficient method, future work could explore time smoothing techniques to improve its temporal consistency. CSP isolated the Cz electrode and modulated time-frequency representations, revealing enhanced low-frequency activity. xDAWN, designed for ERP enhancement, yielded distinct spatial filters and the best performance among all tested filters for our use case. Future work could (i) evaluate non-linear methods to improve performance and (ii) adapt the filters on a per-subject and single-trial basis for online use.

Acknowledgments

This research was funded by the European Union ERANET CHIST-ERA 2020 (CHIST-ERA-20-BCI-003 - “GENESIS”) and the French Research Agency (ANR-21-CHRA-0001-01). Platform equipment was co-financed by the European Regional Development Fund, the State, and the Hauts-de-France Region within the RITMEA project.

References

[1] G. van der Lee, F. Cabestaing, A. Lécuyer, R. Scherer, and H. Si-Mohammed, “EEG Markers of Acceleration Perception in Virtual Reality,” in *Graz Brain-Computer Interface Conference*. Graz, Austria: Verlag der Technischen Universität Graz, Sep. 2024, p. 249.

[2] C. Jutten and J. Herault, “Blind separation of sources, part I: An adaptive algorithm based on neuromimetic architecture,” *Signal Processing*, vol. 24, no. 1, pp. 1–10, Jul. 1991.

[3] K. Fukunaga, *Introduction to Statistical Pattern Recognition*, 2nd ed. Academic Press, 1990.

[4] A. Schurger, S. Marti, and S. Dehaene, “Reducing multi-sensor data to a single time course that reveals experimental effects,” *BMC Neuroscience*, vol. 14, no. 1, p. 122, Oct. 2013.

[5] B. Rivet, A. Souloumiac, V. Attina, and G. Gibert, “xDAWN algorithm to enhance evoked potentials: Application to brain-computer interface,” *IEEE transactions on bio-medical engineering*, vol. 56, no. 8, pp. 2035–2043, Aug. 2009.

[6] S. Akuthota, K. R. Kumar, and J. R. Chander, “A Complete Survey on Common Spatial Pattern Techniques in Motor Imagery BCI,” *Journal of Scientific and Innovative Research*, vol. 12, no. 3, pp. 40–49, Sep. 2023.

[7] L. Farwell and E. Donchin, “Talking off the top of your head: Toward a mental prosthesis utilizing event-related brain potentials,” *Electroencephalography and Clinical Neurophysiology*, vol. 70, no. 6, pp. 510–523, Dec. 1988.

[8] J. C. Ditz, A. Schwarz, and G. R. Müller-Putz, “Perturbation-evoked potentials can be classified from single-trial EEG,” *Journal of Neural Engineering*, vol. 17, no. 3, p. 036008, May 2020.

[9] E. Maris and R. Oostenveld, “Nonparametric statistical testing of EEG- and MEG-data,” *Journal of Neuroscience Methods*, vol. 164, no. 1, pp. 177–190, Aug. 2007.